

A comparison of galaxy group luminosity functions from semi-analytic models

Owain N. Snaith,^{1*} Brad K. Gibson,¹ Chris B. Brook,¹ Stéphanie Courty,^{1,2}
Patricia Sánchez-Blázquez,^{1,3,4} Daisuke Kawata,⁵ Alexander Knebe⁴
and Laura V. Sales⁶

¹University of Central Lancashire, Jeremiah Horrocks Institute, Preston PR1 2HE

²Centre de Recherche Astrophysique de Lyon, Ecole Normale Supérieure de Lyon, Lyon F-69007, France

³Instituto de Astrofísica de Canarias, Vía Lactea S/N, E-38205 La Laguna, Tenerife, Spain

⁴Departamento de Física Teórica, Universidad Autónoma de Madrid, E-28049 Madrid, Spain

⁵Mullard Space Science Laboratory, University College London, Holmbury St Mary, Dorking, Surrey RH5 6NT

⁶Kapteyn Astronomical Institute, PO Box 800, Groningen, the Netherlands

Accepted 2011 April 11. Received 2011 March 23; in original form 2010 May 20

ABSTRACT

Semi-analytic models (SAMs) are currently one of the primary tools with which we model statistically significant ensembles of galaxies. The underlying physical prescriptions inherent to each SAM are, in many cases, different from one another. Several SAMs have been applied to the dark matter merger trees extracted from the Millennium Run, including those associated with the well-known Munich and Durham lineages. We compare the predicted luminosity distributions of galaxy groups using four publicly available SAMs, in order to explore a galactic environment in which the models have not been explored to the same degree as they have in the field or in rich clusters. We identify a characteristic ‘wiggle’ in the group galaxy luminosity function generated using the De Lucia et al. SAM, which is not present in the Durham-based models, consistent to some degree with observations. However, a comparison between conditional luminosity functions of groups between the models and observations suggests that neither model is a particularly good match. The luminosity function wiggle is interpreted as the result of the two-mode active galactic nucleus feedback implementation used in the Munich models, which itself results in flattened magnitude gap distribution. An associated analysis of the magnitude gap distribution between first- and second-ranked group galaxies shows that while the Durham models yield distributions with approximately equal luminosity first- and second-ranked galaxies, in agreement with observations, the De Lucia et al. models favour the scenario in which the second-ranked galaxy is approximately 1 mag fainter than the primary, especially when the dynamic range of the mock data is limited to 3 mag.

Key words: galaxies: clusters: general – galaxies: formation – galaxies: groups: general – galaxies: haloes – galaxies: luminosity function, mass function.

1 INTRODUCTION

In an ideal world, simulating and analysing the formation and evolution of galaxies within Gpc-scale cosmological volumes would be accomplished via the use of self-consistent gravitational N -body and hydrodynamical models. While such an approach is feasible in certain restricted situations, it remains impractical for most applications. Instead, the compromise most widely adopted is based upon the use of semi-analytic models (SAMs). The merger and

assembly histories of galaxies within SAMs are underpinned by high-resolution cosmological N -body simulations, at the ‘cost’ of employing a posteriori ‘semi-analytical’ treatments of the associated baryonic physics.

In all the SAM models explored in this paper galaxy properties are derived using a range of gas infall, radiative cooling, re-ionization, active galactic nuclei (AGN) and supernova (SN) feedback, morphological transformation, dust and spectrophotometry prescriptions. In general, the inclusion of AGN feedback within the SAM reduces the luminosity and stellar mass of the brightest galaxies. SN feedback is effective in low-mass galaxies, where it becomes an important mechanism by which galactic winds are driven and star formation

*E-mail: onsnaith@uclan.ac.uk

is quenched. Thus, SN feedback leads to a reduction in the number of low-luminosity galaxies. Upon merging, the stars and cold gas of a satellite galaxy (an accreting galaxy) are added to the reservoir of the central galaxy (called ‘centrals’ henceforth) of the parent halo. SAMs have reproduced a range of galactic observables, including colours, luminosities and mass functions.

SAMs come in several flavours, and, although the codes share many similar features as outlined above, they also differ in the way in which certain processes, relating to baryonic physics, are implemented (e.g. treatment of SNe and AGN feedback). These lead different SAMs to produce different solutions to the problem of galaxy formation. Some of these differences have been explored at length in the literature, via direct comparison with both empirical *field* and *cluster* galaxy luminosity functions, which are the *extrema* of galaxy environments (Hatton et al. 2003; Mo et al. 2004; González et al. 2005; Bower et al. 2006; Croton et al. 2006). For example, Mateus (2008) found that the Bower et al. (2006), De Lucia et al. (2006) models give different trends for the temporal evolution of galaxy merger rates based on close pair counting. Díaz-Giménez & Mamon (2010) suggest that the Bower et al. (2006), De Lucia et al. (2006) and De Lucia & Blaizot (2007) models reach different conclusions regarding the rate of chance alignment in low-velocity dispersion compact groups (CGs). Recent examples of problems encountered by the SAM approach include the excess of low-mass red galaxies, as identified by Weinmann et al. (2006) and Baldry et al. (2006). A comprehensive review of the SAM approach can be found in Baugh (2006).

What has *not* been explored, thus far, at least in any formal sense, is the impact of these baryonic physics prescriptions upon the resulting luminosity and stellar mass functions for the most *common* of environments, that of galaxy groups. It is to this aim that our current study is focused. Galaxy groups are environments where galactic evolution is happening at a high rate due to the low-velocity dispersion of groups. This means that galaxy–galaxy interactions are more likely than in clusters. In this paper, we examine the outputs of four widely used SAMs applied to the Millennium Run¹ (Springel et al. 2005) in order to quantify the impact of baryonic physics prescriptions upon the resulting compact and loose group (LG) luminosity functions. Two of the models which we examine will be collectively referred to as the ‘Durham models’, being those of Bower et al. (2006, hereafter D_B06) and Font et al. (2008, hereafter D_F08), which is an updated version of D_B06, with a more sophisticated treatment of ram-pressure stripping. We also analyse two ‘Munich models’, being those of De Lucia et al. (2006, hereafter M_D06)/De Lucia & Blaizot (2007) and Bertone et al. (2007, hereafter M_B07), which differs from M_D06 mainly in the SN feedback recipes. A related model by Croton et al. (2006), of which M_D06 is a direct descendant, is also referred to in our study.

After outlining our galaxy group cataloguing procedure, constructed using a classical friends-of-friends (FoF) approach (Section 2), we examine systematically the predicted distributions of the luminosity, and first-to-second-ranked magnitude gaps for both CG and LG of galaxies, for each of the SAMs under consideration (Section 3). We analyse the luminosity distribution of galaxy groups in the different models so that the next generation of SAMs can improve the implementation of galaxy formation physics.

2 MODELS

The SAMs used in our analysis employ the merger trees associated with the Millennium Simulation (Springel et al. 2005), a large N -body simulation corresponding to a significant volume of the visible Universe, and generated using the *Wilkinson Microwave Anisotropy Probe* (WMAP) year 1 cosmology (Spergel et al. 2003).² The simulation used 2160^3 particles in a periodic box of side length $500 h^{-1}$ Mpc, gravitational softening of $5 h^{-1}$ kpc and individual particle masses of $8.6 \times 10^8 M_\odot$; 64 outputs exist within the Millennium data base, ranging from redshift $z = 127$ to 0. The simulation was post-processed using an FoF algorithm (Geller & Huchra 1983), in order to identify density peaks, and then SUBFIND (Springel et al. 2001) was employed to identify substructure and split spuriously joined haloes. This information was then used to build merger trees for the dark matter haloes on to which the SAMs are ‘mapped’.

Before embarking on a discussion of the predicted luminosity functions resulting from the use of the aforementioned SAMs applied to the Millennium merger trees, it is important to summarize briefly the defining characteristics associated with each of the primary SAMs employed here. We will highlight the different ways in which the codes create merger trees, the way in which galaxy positions are defined, the implementation of satellite disruption and accretion and the way in which SN and AGN feedback are implemented.

2.1 Durham models (D_B06; D_F08)

In the Durham models, merger trees are produced in a manner which follows that of Helly et al. (2003), and the properties of these trees are described in Harker et al. (2006). These models account for ostensibly separate haloes which are joined by a bridge of dark matter and hence can be erroneously put in a single halo by FoF algorithms and also account for haloes which are only temporarily joined. Accounting for these effects results in a halo catalogue containing more haloes than in the original FoF catalogue. The merger trees are then constructed from these catalogues by following subhaloes from early times to late times. We note that the merger trees were constructed independently of those in Springel et al. (2005).

The merging of galaxies, and lifetime of satellite galaxies, are derived using the method presented in Benson et al. (2002), which is considerably more sophisticated than the method used in Cole et al. (2000). When dark haloes merge, a new combined dark halo is formed, and the largest of the galaxies contained within is assumed to be the central galaxy, whilst all other galaxies within the halo are satellites. Satellites are then evolved under the combined effects of dynamical friction, and tidal stripping. These effects are modelled analytically. The initial orbital energy and the angular momentum of the satellite upon merging are specified. The orbital energy is set using a constant value of $r_c(E)/R_{\text{vir}} = 0.5$, representative of the median binding energy of satellites, while the orbital ellipticity is chosen to be between 0.1 and 1.0 at random. Given these parameters, the apocentric distance is found, and the orbit equations are integrated at that point. The host and satellite haloes are all assumed to have Navarro–Frenk–White profiles (Navarro, Frenk & White 1996), while galaxies are modelled as a disc plus spheroid. The satellite galaxies plus halo are then advanced by calculating the combined gravitational forces of the host and satellite

¹ The simulation was carried out by the Virgo Supercomputing Consortium at the Computing Centre of the Max Planck Society in Garching and recovered from <http://galaxy-catalogue.dur.ac.uk:8080/Millennium/>.

² ($\Omega_m, \Omega_b, \Omega_\Lambda, h, n, \sigma_8$) = (0.25, 0.045, 0.75, 0.73, 1, 0.9).

haloes, as well as the effects of dynamical friction, calculated using Chandrasekhar's formula. The code keeps track of tidal stripping to remove mass from the satellites. The new halo mass is then used for the next iteration of the orbit equations.

This integration of the orbital equations continues until one of the three conditions is met: (i) the final redshift, (ii) the host merges with a new larger halo, in which case the satellite becomes a part of the new halo and has new orbital parameters assigned or (iii) the satellite merges with the central galaxy. In this last case, merging takes place when the orbital radius falls below R_{merge} , which is the sum of the half-mass radius of the central and satellite galaxies. The mass of the merged satellite is then added to the central galaxy. The merging times largely match those of Cole et al. (2000); however, some satellites have very long merging times, as they lose a great deal of mass through tidal stripping, meaning that dynamical friction forces become very weak.

The Durham models relate SN reheating directly to the circular velocity of the galaxy disc according to Cole et al. (2000):

$$\dot{M}_{\text{reheat}} \propto V_{\text{disc}}^{-2} \dot{M}_*, \quad (1)$$

where \dot{M}_{reheat} is the rate of change of the mass of the reheated gas, V_{disc} is the disc's circular velocity, \dot{M}_* is the time derivative of stellar mass and \dot{M}_{eject} is the change in the mass of the ejected gas. In haloes with a shallow potential, this has the effect of reducing the amount of the cold gas available to form stars by heating the gas back into the hot-gas reservoir. The hot gas is dominated by ejection for low-mass haloes and by reheating without ejection for large haloes. For low-mass galaxies, SN feedback is an important mechanism by which galactic winds are driven and star formation is quenched.

The Durham models implement AGN feedback in such a way as to regulate the cooling of the hot gas. In large haloes with large Eddington luminosity, the AGN feedback is assumed to balance heating and cooling, thus truncating star formation. This prevents the formation of overluminous galaxies. While feedback is active, the black hole is assumed to grow proportionally to the cooling luminosity, and the gas is accreted due to disc instabilities. The model assumes quasi-hydrostatic cooling for AGN active galaxies and has a strict transition between AGN 'active' and 'inactive' phases. AGN feedback becomes efficient in galaxies of mass greater than $\sim 2 \times 10^{11} h^{-1} M_{\odot}$.

The essential difference in the D_B06 and D_F08 models is the implementation of ram pressure stripping of the hot gas. In the D_B06 model, along with both Munich models, the hot gas is instantaneously stripped when it enters a halo already containing a central galaxy. In the D_F08 model, this process happens gradually and depends on the orbit of the galaxy. This has the effect of reducing the population of faint red galaxies.

2.2 Munich models (M_D06; M_B07)

The Munich merger trees (Springel et al. 2005) used in M_D06 and M_B07 follow the positions of subhaloes for as long as they can be identified. Identification is possible only when the number of particles bound to a subhalo exceeds the minimum number of particles set by `SUBFIND`. The trees are constructed by following the most bound halo particles and searching for the descendant halo in the next output.

One of the key differences between the Munich models and those of Durham is that the Munich models explicitly follow dark matter haloes even after they are accreted on to larger systems, allowing the dynamics of satellite galaxies residing in the infalling haloes

to be followed until the dark matter substructure is destroyed. The galaxy position is calculated by assigning the galaxy to the most bound particle of a (sub)halo at each time step. This is done until the (sub)halo is no longer identifiable, whereupon the galaxy is assigned to the most bound particle of the (sub)halo at the last time the (sub)halo could be identified. An analytic countdown to galaxy merging begins when the satellite subhalo can no longer be identified and resets if the parent halo undergoes a major merger. Thus, in the Munich models, the lifetime of galaxies in groups depends on the amount of time the (sub)halo finder can identify the subhalo plus the analytic countdown. The analytic merging follows that of Croton et al. (2006):

$$\tau_{\text{mrg}} = 1.17 \frac{V_{\text{H}} r_{\text{sat}}^2}{G m_{\text{sat}} \ln \left(1 + \frac{M_{\text{H}}}{M_{\text{sat}}} \right)}, \quad (2)$$

where $\ln(1 + \frac{M_{\text{H}}}{M_{\text{sat}}})$ is the coulomb logarithm, V_{H} is the halo circular velocity, r_{sat} is the distance of the subhalo from the halo centre at the time it is last identified, m_{sat} is the mass of the satellite dark halo at the time it was last identified and M_{H} is the halo mass.

In M_D06, the amount of the reheated (by SNe) cold gas is proportional to the stellar mass, and the mass ejected from the halo is inversely proportional to the host halo's circular velocity squared (Croton et al. 2006):

$$\dot{M}_{\text{reheat}} \propto V_{\text{vir}}^{-2} \dot{M}_*, \quad (3)$$

The important parameters, V_{vir} and M_* , have the same relationship in the Durham models. In the Munich models, the reheated mass is proportional to the mass of the halo, while in the Durham model it is proportional to the disc mass. The M_B07 model adopts a more sophisticated treatment of SN feedback. Rather than simply parametrizing the effect of SN feedback, the M_B07 model follows the dynamical evolution of the wind as an adiabatic expansion followed by snowploughing. This implementation has the effect of increasing the luminosity of the brightest galaxies. As also occurs with the Durham models, some of the gas will be ejected from low-mass haloes in both Munich models.

In the Munich models, a two-mode formalism is adopted for the AGN, wherein a high-energy, or 'quasar' mode occurs subsequent to mergers, and a constant low-energy 'radio' mode suppresses cooling flows due to the interaction between the gas and the central black hole (Croton et al. 2006). In the quasar model, accretion of gas on to the black hole peaks at $z \sim 3$, while the radio mode reaches a plateau at $z \sim 2$. AGN feedback is assumed to be efficient only in massive haloes, with SN feedback being more dominant in lower mass haloes.

The properties of groups in the Munich models, M_D06 and M_B07, are similar to each other in many cases as are the properties of the two Durham models: D_B06 and D_F08. Thus, in some analysis, we just discuss the M_D06 and D_B06 models, as representatives of their models' lineages. We only discuss the results based on their descendants, M_B07 and D_F08, when they show significantly different behaviour from M_D06 and D_B06.

3 GROUPS

In order to construct a statistically significant (and representative) galaxy group catalogue, we have worked with a set of subsamples of the Millennium Simulation, each amounting to ~ 3 per cent of the available volume – specifically, 64 boxes of side length $125 h^{-1}$ Mpc drawn from the data base. Our results are robust to the arbitrary selection of the box and having been tested a posteriori on alternate boxes of equal size. A luminosity limit of $M_r = -17$ in the

Sloan Digital Sky Survey (SDSS) r band was imposed. At lower luminosity, the effect of the limited mass resolution of the N -body background affects the completeness of the sample. We identify galaxy groups as overdensities in the galaxy population using an FoF algorithm (Geller & Huchra 1983). No maximum number of members is set, but we require that at least four galaxies are linked in order to define a group. Although this removes groups such as the Local Group, it follows the Hickson (1982) definition of CGs.

We first construct an 'LG' catalogue using a linking length of 0.2 times the mean interparticle separation (or in this case, intergalactic separation). We made this choice by assuming that the galaxies follow the dark matter. This corresponds to a comoving linking length of $\sim 500 h^{-1}$ kpc. To examine the effects of density we also define two 'compact group' catalogues – CG and very compact group (vCG) – using comoving linking lengths of 150 and $50 h^{-1}$ kpc, respectively. The CG linking length of $150 h^{-1}$ kpc is similar to that advised by McConnachie, Ellison & Patton (2008), based upon their 3D linking-length analysis from mock catalogues of Hickson CGs based on M_D06. The vCG linking length is comparable to the projected linking length used by Barton et al. (1996) and Allam & Tucker (2000) to identify groups, a value arrived at by calibrating to the Hickson et al. (1992) catalogue using projected galaxy separations.

We note that the CG galaxies are, by necessity of the group finding algorithm, subsets of the LG catalogue, in that every galaxy assembled into a group at short linking length must be a part of a group with a larger linking length. Our catalogues also contain clusters and cluster cores, a point to which we return shortly. The physical interpretation of the linking-length variation and its impact upon resulting galaxy distribution is non-trivial. The FoF algorithm essentially probes deeper into the potential well at shorter linking lengths, selecting only galaxies closer to the cluster/group core. These galaxies are generally old, and have sunk deeper into the cluster potential, or they are galaxies near their respective orbital pericentre.

The algorithm does not only extract the inner region of groups. Galaxies in the outskirts of clusters that happen to be close to one another can also be linked together. This may either be due to a temporary alignment of galaxies that are simply 'passing through' that region, or because the galaxies were in close proximity before they entered the cluster, and have not yet been disburbed by tidal forces. These peripheral groups are essentially cluster substructure and are a natural part of the analysis. Peripheral groups represent a small fraction of LGs, but represent ~ 20 per cent of CGs and vCGs. Also worth noting is that the linking length adopted for LGs means that the group can include galaxies from beyond the limit of the dark matter halo occupied by the majority of group member galaxies. This means that our LG catalogue is not exactly equivalent to groups that are defined by the halo occupation of galaxies.

3.1 Merging time-scales

We compare the merging histories and time-scales of haloes and galaxies within the models. Any differences will be important in determining the origin of the properties of various groups. To compare the lifetime of satellites we look at (a) the lifetimes of satellites that have merged and thus contribute to the mass and luminosity of the central galaxy and (b) the lifetime of satellites that have not yet merged, and are hence satellites at $z = 0$, and contribute to the group catalogues.

Fig. 1 shows the distribution of merging times, defined as the time between a satellite first entering a halo and being totally merged with

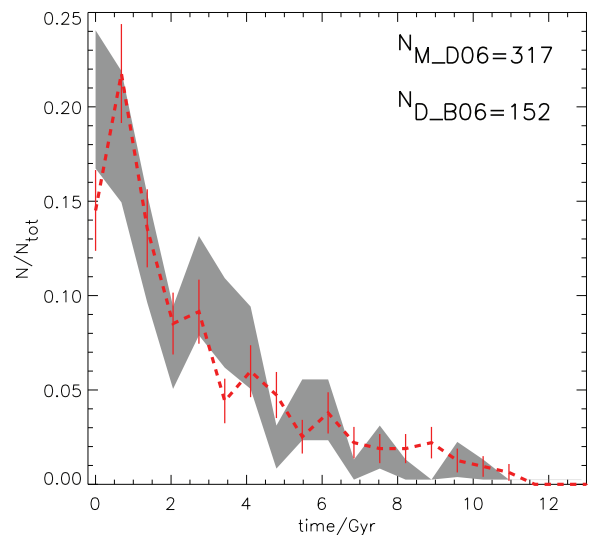


Figure 1. The distribution of galaxy-merging times. The y-axis is the number of galaxies in each bin normalized by the total number of galaxy mergers. The black line is for the D_B06 model and the red dotted line is for the M_D06 model. Errors are Poisson. The number of merging galaxies in each model is quoted in the panel.

the central galaxy. We select the same 19 Millennium Simulation clusters from each model to make a fair comparison between the codes and do not put any limit on the luminosity of infalling satellites. The distribution of merging times shows little difference between the models. The average M_D06 satellite has lasted 5.8 Gyr, while D_B06 satellites have lasted 6.2 Gyr, with standard deviations of ~ 1 . We note, however, that twice as many satellites have merged in the Munich model (317) than in the Durham model (152).

This result seems to be a little contradictory as similar merging time-scales should result in similar numbers of mergers. We look to the number of satellites that do not merge in order to reconcile this. Fig. 2 shows the time of infall for the satellites into the host halo: for satellites that merge (panel A), satellites that do not merge but

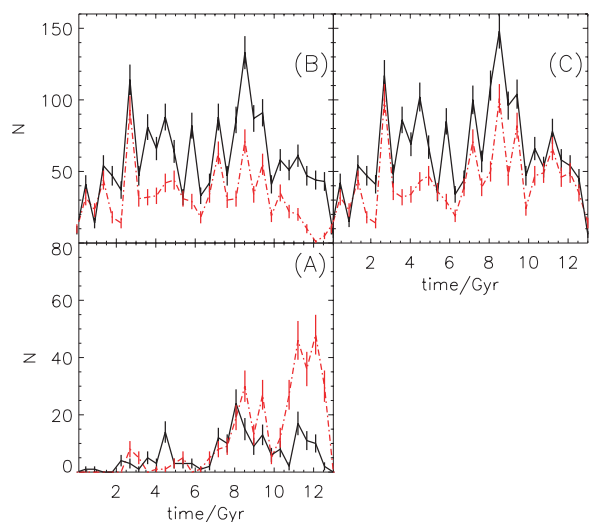


Figure 2. Panel A: the number of galaxies which merge with the halo central galaxy during the simulation against the time the galaxy entered the host halo. Panel B: the infall time of those galaxies which are still satellites at $z = 0$. Panel C: the sum of the plots in panels A and B. The solid black line shows the D_B06 result and the red dashed line is for M_D06.

rather remain as satellites at $z = 0$ (panel B) and all the satellites (panel C). Again, the fact that more satellites merge in M_D06 compared with D_B06 can be seen in panel A, but it can also be seen that the difference is dominated by satellites which fall into the host halo at early times. By contrast, the number of satellites that do not merge at all is significantly larger for D_B06, compared with M_D06. The difference is greatest for satellites which accrete early. This significant population of satellites that do not merge by $z = 0$ can be expected to affect the properties of groups which we present in the remainder of this study, both because of the lower number of satellites ‘feeding’ the central galaxy in D_B06, and also the larger numbers of satellites that survive to be included in the group catalogues. Panel C shows the infall time of all satellites from our sample of 19 clusters, regardless of whether they merged, and shows that the differences between the models being relatively minor.

There are more haloes falling into the Durham models and fewer galaxy mergers. The galaxies *which merge* have the same lifetime in each model. If we look at the time of infall of galaxies which merge, and those that remain in the cluster at $z = 0$, (Fig. 2), there is a substantial population of galaxies which never merge. In the Durham models, more galaxies survive than those in the Munich models (panel B of Fig. 2). Furthermore, we also see that more (of the early accreted) galaxies merge with the central object in the Munich model (panel A of Fig. 2). At the earliest times in the M_D06 model almost all the galaxies have merged, while in the D_B06 model they have not. Thus, the ‘maximum’ lifetime of satellite galaxies is 10 Gyr in M_D06 but > 13 Gyr in D_B06.

While not shown, our examination of the merger trees also found that in the D_B06 model a greater number of haloes merge with the 19 clusters. This is because subhaloes are not followed when constructing the merger trees in the Durham models. In the Munich models, there is a delay in the halo merger time relative to the Durham models because infalling haloes are able to enter the subhalo stage before they are considered merged. When the (sub)halo in each model is no longer identifiable, the SAMs are used to calculate the lifetimes of galaxies. In the Durham models, there appears to be an extremely long lived population of satellites which are not present in the Munich SAMs.

4 OBSERVATIONS

We use the observational LG catalogues of Tago et al. (2008), Yang, Mo & van den Bosch (2008) and Tucker et al. (2000), and the CG catalogue of Allam & Tucker (2000). These group catalogues take large redshift surveys of galaxies and use an FoF algorithm to assemble them into groups. Tago et al. (2008, SDSS5_T08) implemented a standard FoF algorithm which scales according to the distance and applied it to the SDSS Data Release 5 (DR5; Adelman-McCarthy et al. 2007). The initial linking length is $0.25 h^{-1}$ Mpc in projection and 250 km s^{-1} along the line of sight. The Tucker et al. (2000, LCRS_T00) catalogue uses the Las Campanas Redshift Survey (LCRS; Shectman et al. 1996) and applies a fiducial linking length of $0.715 h^{-1}$ Mpc and 500 km s^{-1} , scaled from this value at $z = 0.1$ and rising to 1.8 times this at $z = 1.7$. Allam & Tucker (2000, LCRS_A00) uses the same catalogue as LCRS_T00 but a shorter linking length of $0.05 h^{-1}$ Mpc and 500 km s^{-1} . Finally, Yang et al. (2008, SDSS4_Y08) use a more complicated iterative approach, which, nevertheless, includes an FoF algorithm at its core (Yang et al. 2005). This algorithm applied to SDSS DR4 (Adelman-McCarthy et al. 2006).

Our synthetic group catalogues are compared directly with these empirical data sets wherever such comparisons are possible and meaningful within our analysis, bearing in mind limitations in the models, and in the observations. Where appropriate, ‘cuts’ are made in the synthetic catalogues to mimic observations.

5 RESULTS

5.1 Density of groups in the models

The difference in the proportion of galaxies in groups should provide a key diagnostic for comparing and discriminating between the four SAMs, relative to empirical data. Within the Millennium Simulation volume at $z = 0$, the four SAMs under consideration yield differing numbers of galaxies, despite being built upon the same underlying dark matter distribution. It is useful to review the respective galaxy numbers and distributions for these models. Restricting the discussion to the relevant sampling criteria (i.e. $M_r < -17$) the M_D06 and M_B07, and D_B06 and D_F08 models have a galaxy number density given in Table 1. The number density of galaxies is quite similar in the field for each model as well as in LGs. However, the Durham models have significantly denser galaxy populations within CGs and vCGs. The physics, which the different models employ to account for group environments, appear to have significantly altered the nature of CGs.

The relative proportion galaxies that are classified as being the members of groups, along with the average group richness, are listed in Table 2. In this instance, we define group richness as simply being the number of galaxies in a group.

The percentage of galaxies associated with LGs (and the numbers of galaxies per LG) is comparable between three of the four SAM variants, with the M_D06 model showing approximately 6 per cent fewer groups than the D_B06 model. The models diverge increasingly with decreasing linking length, with the Munich models, M_D06 and M_B07, having 5–6 times fewer vCGs than in the

Table 1. The number density of field galaxies and LG, CG and vCG for the D_B06, M_D06, M_B07 and D_F08 models.

	D_B06 ($h^3 \text{ Mpc}^{-3}$)	D_F08 ($h^3 \text{ Mpc}^{-3}$)	M_D06 ($h^3 \text{ Mpc}^{-3}$)	M_B07 ($h^3 \text{ Mpc}^{-3}$)
Field	6.5×10^2	6.6×10^2	6.3×10^2	5.0×10^2
LG	2.1×10^3	2.2×10^3	2.0×10^3	1.6×10^3
CG	1.3×10^3	1.4×10^3	8.9×10^4	8.7×10^4
vCG	5.4×10^4	6.6×10^4	1.2×10^4	1.4×10^4

Table 2. First four rows present the percentage of galaxies in FoF groups for LG, CG and vCG in each of the four SAMs, while the later rows show the mean group richness for groups in the four models.

	LG	CG	vCG
Bower (D_B06)	44	18	5.5
Font (D_F08)	44	19	6.0
De Lucia (M_D06)	38	10	0.9
Bertone (M_B07)	43	14	1.3
Bower (D_B06)	13.5	9.4	6.6
Font (D_F08)	13.1	9.2	6.6
De Lucia (M_D06)	11.5	7.5	4.7
Bertone (M_B07)	13.6	8.0	5.0

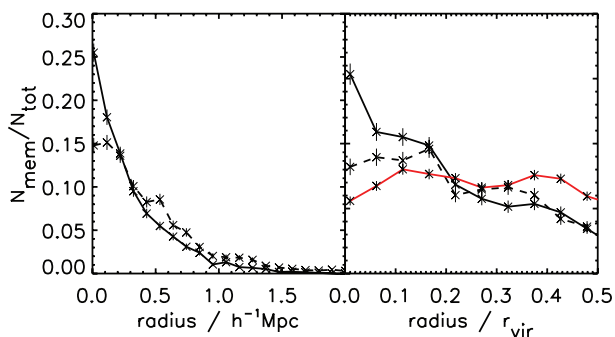


Figure 3. Left-hand panel: the number of galaxies in LGs against the distance from the centre, normalized by the total number of galaxies. The solid line is for D_B06 LGs and the dashed line is for M_D06 LGs. Right-hand panel: the normalized number of galaxies against the radius scaled by the virial radius of the host. The red line shows SDSS4_Y08 LGs for the 60 most massive clusters. Errors are Poisson. There are 2294, 2022 and 4688 in the D_B06, M_D06 and SDSS4_Y08 data sets, respectively.

Durham models. The M_D06 model produces noticeably fewer rich groups at all linking lengths compared with the other Munich model, M_B07. This indicates that the implementation of SNe has a significant effect on the richness of group catalogues. The Durham models, D_B06 and D_F08, have slightly richer LGs than the Munich models. This is associated with the smaller populations of medium brightness red galaxies in the Munich models, which may be the result of the differences in the creation of halo catalogues, the tracing of subhalo mergers, or due to radio mode AGN feedback.

McConnachie et al. (2008, 2009) compared CGs in mock redshift catalogues to SDSS DR6 observations and concluded that the M_D06 SAM overproduces CGs by ~ 50 per cent. By extension, Table 2 indicates that the D_B06 and D_F08 models result in an even more dramatic ‘overproduction’ of CGs (by an order of magnitude). Thus, in this regime, none of the models is a good fit to the empirical data, and the Durham models are particularly poor.

Fig. 3 shows the galaxy distribution of galaxies with radius for the LGs of M_D06 and D_B06 models. The left-hand panel shows the number of satellites versus radius in Mpc. The right-hand panel of Fig. 3 shows the same plot with the radius scaled by the virial radius. Both panels show that there are more satellites in the inner regions of the D_B06 LGs, relative to the outer regions, compared with the M_D06 model. The red line in the right-hand panel shows the 60 most massive SDSS4_Y08 observed LGs, making them similar in the mass range to the population used in making the simulation plots. This indicates that both models have a radial distribution of satellites which is more centrally concentrated than the observations, with the problem being particularly acute in the D_B06 model.

This more concentrated distribution of satellites is also reflected in the distribution of nearest neighbour pair separation distances for LG members, as shown in Fig. 4. It can be seen that the nearest neighbour separation for the D_B06 model is smaller than for the M_D06 and M_B07 models. We note that the D_F08 model groups have very similar properties to D_B06 and are thus not included in these figures.

5.2 Luminosity functions

We now plot the group luminosity functions. Fig. 5 shows how the luminosity function changes in the different group environments for the SAM models. It is unsurprising that the global luminosity functions of all the models are similar, because the SAMs are designed

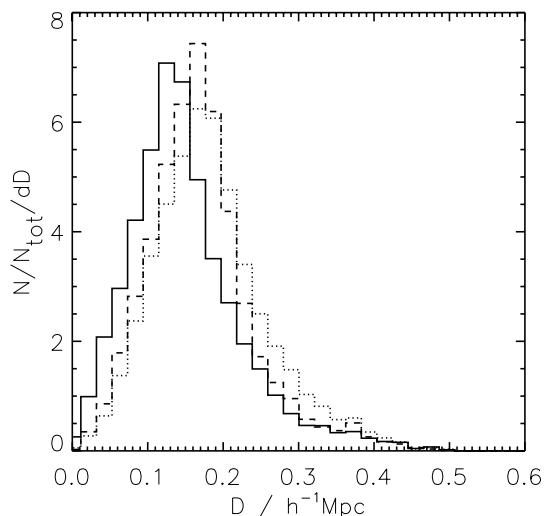


Figure 4. The distribution of the nearest neighbour pair separations for galaxies in LGs for the three models, the solid line is D_B06, the dashed line is M_D06 and the dotted line is D_B07. The plot shows that D_B06 galaxies tend to be closer together on average.

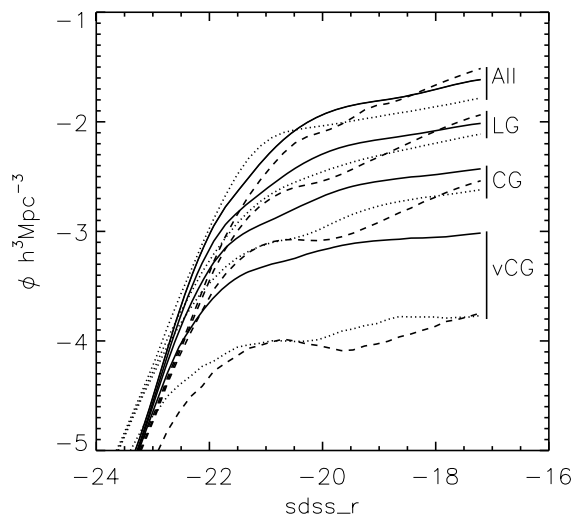


Figure 5. Derived SDSS r -band luminosity functions for galaxy groups constructed with the SAMs described herein: ‘All’ refers to the global galaxy luminosity function; ‘LG’ refers to loose groups; ‘CG’ refers to compact groups and ‘vCG’ refers to very compact groups. The solid/dashed/dotted lines refer to the D_B06/M_D06/M_B07 models, respectively.

to replicate the same observational luminosity function of Blanton et al. (2003). At smaller linking lengths (moving from top to bottom in the figure) there is a decreasing number of galaxies in all SAMs, a fact which is more dramatic in the Munich variants, as noted in Section 5.1. This provides further evidence that the Durham model galaxies are more centrally concentrated than those of the Munich variants.

The second feature of Fig. 5 is the relative dearth of intermediate-luminosity ($-21 \lesssim M_r \lesssim -18$) galaxies in the M_D06 catalogues (in relation to a simple Schechter 1976 function). This is manifest in the ‘wiggle’ or ‘dip’ seen in the M_D06 group luminosity function. This feature is not present in other models. This wiggle becomes more apparent at shorter linking lengths (i.e. CGs and vCGs). The M_B07 SAM, which employs the same AGN feedback prescription as M_D06, shows no such feature in the luminosity function.

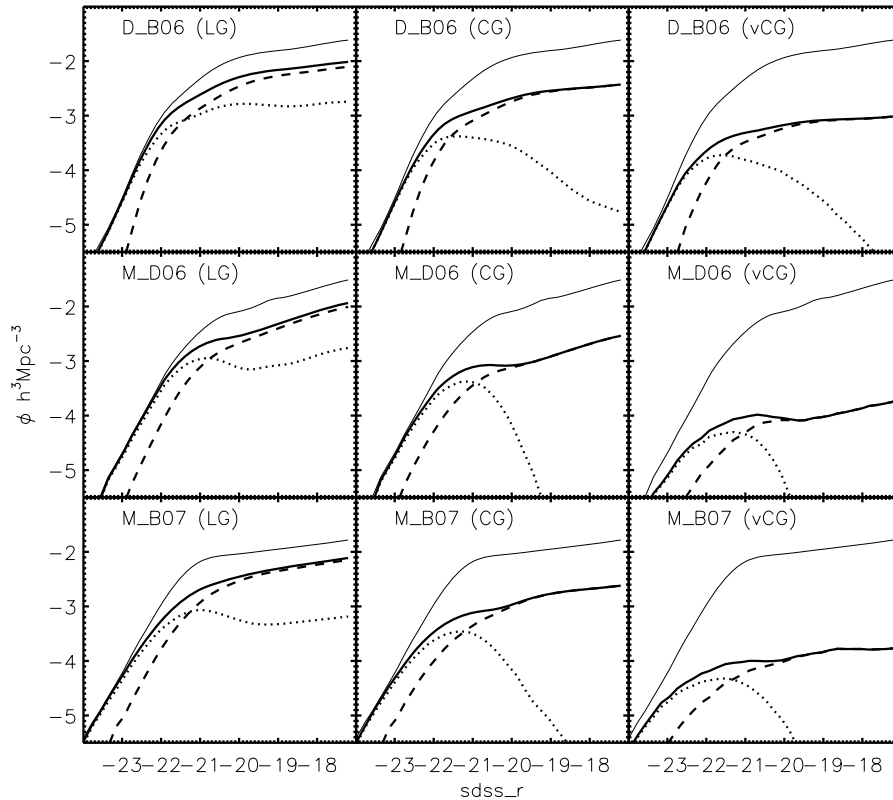


Figure 6. Group luminosity functions for the three primary SAMs under consideration (D_B06, M_D06 and M_B07). In each panel, the dotted lines correspond to the central galaxies and the dashed lines are for the satellites; the thick solid lines represent the group luminosity function and the thin solid line defines the global galaxy luminosity function for reference. The legends D_B06, M_D06 and M_B07 refer to the models as defined above and the number in brackets refers to the linking length in h^{-1} kpc, so the left-hand column is for LGs, the centre column is for CGs and the right-hand column is for vCGs.

Weinmann et al. (2006, fig. 3) show a similar wiggle in the luminosity function of groups in particular mass bins, i.e. the conditional luminosity function, using the Croton et al. (2006) SAM, which is a close ‘cousin’ to the M_D06 SAM employed here.

In order to better understand the origin of the shape of these luminosity functions, we decompose the luminosity functions of the three primary SAMs (D_B06, M_D06 and M_B07) and the three primary linking lengths (LG, CG and vCG) under consideration here, into central galaxies and satellites (Fig. 6). The global galaxy luminosity function is also shown for reference. The M_D06 (middle row) and M_B07 model (bottom row) centrals show a Gaussian distribution, while the D_B06 model (top row) centrals are better described by a Schechter function. There is an increase in the number of faint central galaxies in LGs compared with CGs and vCGs, which alters the shape of the central luminosity function as we move to larger linking lengths. All satellites are distributed roughly according to Schechter functions.

The wiggle in the M_D06 luminosity function is due to the combined effect of (i) a general lack of satellites and (ii) the ‘peaked’ nature of the central galaxy luminosity distribution. Relative to the D_B06 SAM prediction, this distribution of centrals is very narrow, without the low-luminosity tail associated with the D_B06 model. This effect is particularly apparent at the shortest linking lengths, i.e. in vCGs. The greater total number of vCGs in the Durham models compared to the Munich models is also clear in the vCG panels, again reflecting their central concentration.

The contrast between the M_D06 and M_B07 models is of particular interest because they use the same AGN feedback implementation but differ in their choice of SN feedback. The more

sophisticated and more effective SN model of M_B07 makes the luminosity distribution of centrals wider by making a tail towards fainter magnitudes that is not present in M_D06. The most luminous galaxies are also more luminous in M_B07 than in M_D06. The M_B07 treatment leads to a more significant population of intermediate-luminosity satellites with a shallower luminosity function, thus smoothing the wiggle. A lower number of low-luminosity satellite galaxies in such a shallow luminosity function is accompanied by ‘overluminous’ massive (luminous) galaxies (M_B07). M_B07 shows a decrease in the number of low-luminosity satellites, reflecting an SN feedback in M_B07 which is stronger in dwarfs and weaker in large haloes. The increase in high-luminosity galaxies and decrease in low-luminosity galaxies are noted in M_B07, which they suggest could be solved by increasing the SN feedback time or increasing the effect of AGN feedback. It also produces a wider central galaxy distribution by not only increasing the number of very bright galaxies but also by increasing the population of dim centrals.

5.3 Brightest group galaxy

We define three types of identified groups. The first type, bright central groups (BCGs), are those where the brightest galaxy is also the central. The second type, peripheral groups, are those without a central galaxy and, therefore, the brightest galaxy is a satellite. The third type of group, dim centrals, are those where the central galaxy is not the brightest. Except in the D_F08 model, the central galaxy is the only one with hot gas and it acquires all the hot gas from

Table 3. Proportion of galaxy group types where the first number is the proportion of bright central, peripheral and dim central groups.

Model	LG	CG	vCG
D_B06	79/00/21	63/12/25	64/15/21
M_D06	90/01/09	74/21/05	75/20/05
M_B07	82/02/16	70/22/08	71/23/06

infalling satellites. The central galaxy is also the only galaxy that experiences mergers and grows hierarchically. Table 3 shows the populations of these three types for LG, CG and vCG, the format being, groups with BCGs/peripheral groups/dim central groups.

There is a difference between the three main models for LGs. The Durham models have a smaller fraction of BCGs relative to dim centrals, compared with the Munich models. This discrepancy continues to smaller linking lengths. It is likely that the greater number of mergers in the Munich model feed the growth of the central galaxy. The more sophisticated SN feedback of the M_B07 model has decreased the fraction of BCGs. The Munich models also have more peripheral groups at all linking lengths.

In Fig. 7 the luminosity functions of the first-ranked galaxies (i.e. the brightest galaxy in each group) of our groups have been plotted. These have then been decomposed by group type, with distribution of first-ranked galaxies in BCGs, the first-ranked galaxies in peripheral groups and the first-ranked galaxies in dim central groups. It can be seen that, in the Munich SAMs, for the denser groups, there is a large difference between the shape of the LF of the brightest galaxies in central and peripheral groups. The difference is most

extreme for the M_D06 model, where the low-magnitude tail is due, almost entirely, to peripheral groups. In contrast, in the D_B06 model the distribution of groups is not particularly different for the different group types.

5.4 Halo-based groups

In this section, groups consist of galaxies which lie within the same dark matter halo, whose extent is determined by using a density contour defined by a dark matter particle separation of 0.2 times the mean interparticle separation. This is not to be confused with the linking length used to defined groups which acts on galaxies rather than dark matter particles. Groups determined in this manner differ from those determined by using FoF algorithms. Even for LGs there is not a one-to-one correspondence between halo groups and FoF groups. The limit on the minimum number of galaxies used to define a group remains at 4.

We examine the conditional luminosity functions in three different group mass bins. These conditional luminosity functions are plotted in Fig. 8 for the D_B06, M_D06 and M_B07 SAMs. The luminosity functions are further separated into centrals (middle row) and satellites (bottom row).

The 10^{13-14} and $10^{14-15} M_{\odot}$ mass bins show little evidence for the ‘wiggle’ (for any of the SAMs). The ‘wiggle’ in the M_D06 model, and to a lesser extent the M_B07 model, is particularly prominent in the lowest mass bin (top-right panel), where a number of physical processes become relevant. Bower et al. (2006) point out that at $\sim 2 \times 10^{11} M_{\odot}$ the cooling rate exceeds the free-fall rate and the halo is no longer in hydrostatic equilibrium. This has repercussions for the effectiveness of feedback from the central source (Binney 2004) and is used in the Durham paper to explain

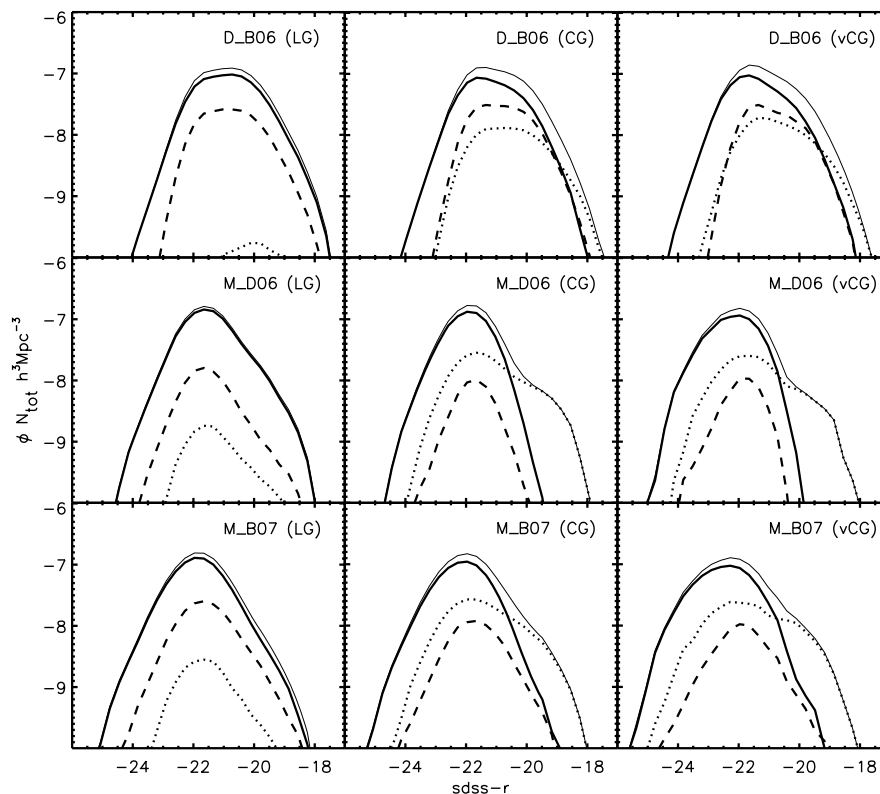


Figure 7. Luminosity function of all first-ranked galaxies (the brightest galaxy in each group, thin solid line); distribution of first-ranked galaxies in bright central groups (thick solid line); the first-ranked galaxies in peripheral groups (dotted line) and the first-ranked galaxies in dim central groups (dashed line).

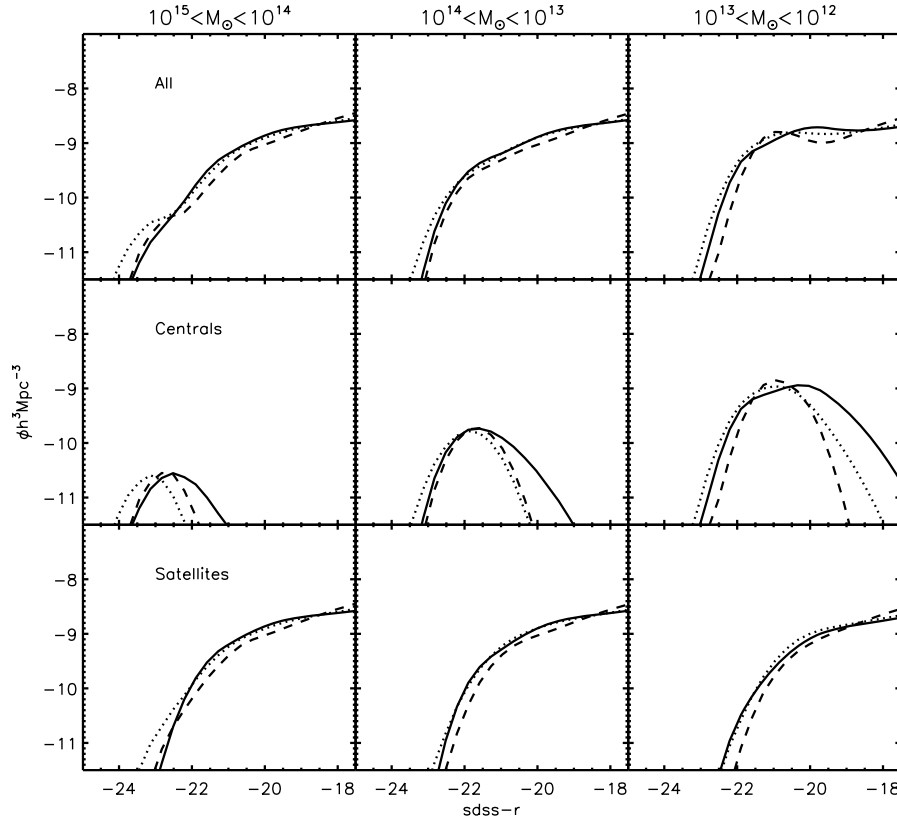


Figure 8. The conditional luminosity functions in three mass bins which correspond roughly to clusters, large groups and small groups, for halo-based groups for the three primary SAMs employed here, at redshift $z = 0$. The top row shows the distributions of all halo members, the second row shows the central galaxies and the bottom row shows the satellites. The solid, dashed and dotted lines are for the D_B06, M_D06 and M_B07 models, respectively.

the break in the luminosity function. Our results indicate that in the Munich models the processes occurring in that mass range may have other repercussions.

For the highest mass bin, we can see that the satellite luminosity function is steepest for the M_D06 SAM and shallowest for the D_B06 model. The characteristic luminosity at the ‘knee’ of the Schechter function (M_*) is the lowest for the D_B06 model. However, this bin has only a small effect on the ‘wiggle’ alluded to in Section 5.2, which occurs at lower luminosity than the wiggle seen in this particular mass bin. In the $10^{12}–10^{13} M_\odot$ bin, where the wiggle is prominent in the M_D06 model, the satellite distribution is fairly steep and the central galaxy luminosity function is relatively narrow and bright. By contrast the D_B06 model has a much broader central galaxy luminosity function, indicating a tendency to produce significantly more low-luminosity centrals compared to M_D06. Again, the unmerged satellites in the Durham models mean less feeding of the central galaxy resulting in this tail to lower luminosities.

In order to compare this with observations we overplot the results of M_D06 and D_B06 on to the conditional luminosity functions provided by SDSS4_Y08. Weinmann et al. (2006) note that the method used by SDSS4_Y08, presented in Yang et al. (2005), artificially narrows the central galaxy luminosity function. This is because their iterative technique uses the brightest galaxy luminosity in the derivation of the group halo mass, while in the models there is no such direct linking of mass and luminosity. However, the difference is not enough to affect our comparison. SDSS4_Y08 shows the CLFs for groups using SDSS DR4 galaxies and are fitted with modified Schechter and Gaussian functions to the satellite and

central galaxy luminosity distributions, respectively. The functional forms of the fits are

$$\Phi_{\text{cen}}(L|M) = \frac{1}{\sqrt{2\pi}\sigma_c} \exp\left[-\frac{(\log L - \log L_c)^2}{2\sigma_c^2}\right], \quad (4)$$

$$\Phi_{\text{sat}}(L|M) = \phi_s^* \left(\frac{L}{L_s^*}\right)^{(\alpha_s^*+1)} \exp\left[-\left(\frac{L}{L_s^*}\right)^2\right], \quad (5)$$

where L is the luminosity, L_c is the mean position of the Gaussian, σ_c is the width of the Gaussian, ϕ_s^* is the normalization of the modified Schechter function, α_s^* is the low-mass slope and $\log(L_s^*) = \log(L_c^*) - 0.25$ and is the position of the knee of the modified Schechter function.

SDSS4_Y08 provide the best-fitting parameters, which we compare to the M_D06 and D_B06 models using the same mass bins as SDSS4_Y08 in Figs 9(a) and (b), where ‘panel a’ shows the satellite galaxy distribution and ‘panel b’ shows the central galaxy distribution. The highest mass bin in the models corresponds most closely with the observations.

The shapes of the conditional luminosity functions for the satellites are considerably different for the CLFs. At all masses, there are far fewer low-luminosity satellites in the models than in the observations. The discrepancy is less severe for the M_D06 model for high-mass clusters. The difference between observations and models for the satellite luminosity function is larger as we go to lower mass. As we go to $10^{12.75} M_\odot$ and below, it is the D_B07 groups which have more low-luminosity satellite galaxies.

The central galaxy conditional luminosity functions also differ significantly between models and observations. The M_D06

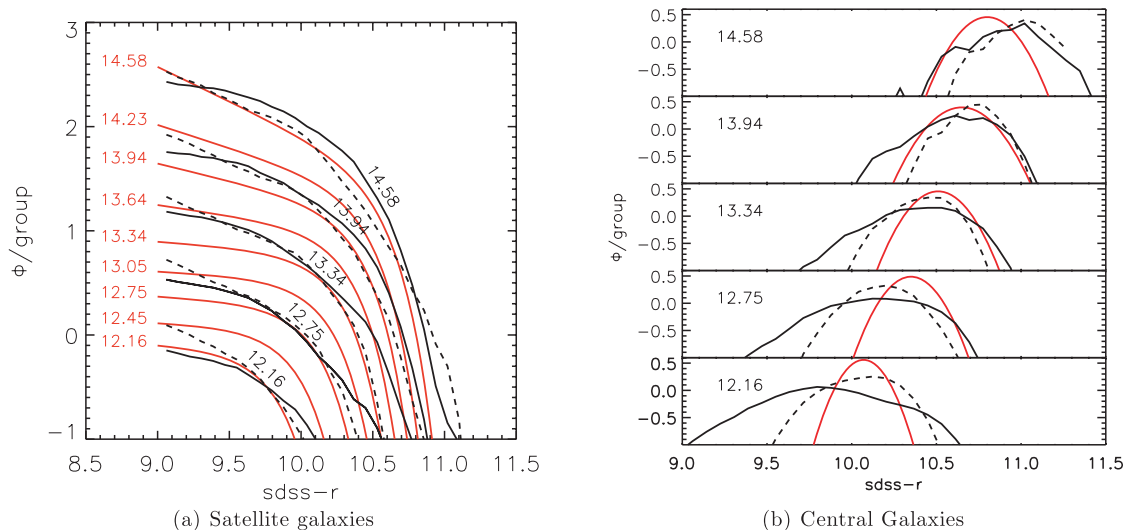


Figure 9. The conditional luminosity function of the models, D_B06 (solid black line) and M_D06 (dashed line) plotted over the CLFs of SDSS4_Y08 (shown in red). The number quoted being the centre of each mass bin and the box width being ~ 0.31 mag. In panel ‘a’ the top pair of lines are the $10^{14.58} M_{\odot}$ cut, the next is the $10^{13.94} M_{\odot}$ cut etc., down to $10^{12.16} M_{\odot}$.

model shows that the low-mass ($10^{12.16} M_{\odot}$) group centrals peak in the same place as the observations, while the mass bins are somewhat displaced, both towards lower luminosities ($10^{12.75}$ and $10^{13.3} M_{\odot}$) and higher luminosities ($10^{13.94}$ and $10^{14.58} M_{\odot}$). The M_D06 model is also broader than the observations. These discrepancies are even greater for the D_B06 groups, which are even wider than the M_D06 groups.

The median vCG has a mass of $1.7 \times 10^{13} M_{\odot}$ for both M_D06 and D_B06, but with considerable variation. This means that the distributions closest to this value are more important to the analysis of vCGs than further away. In Figs 9(a) and (b) we see that the models are reasonably similar at this point, although the peak in the central luminosity function is greater in the Munich variant. This suggests that the significant lack of vCGs in M_D06 compared to D_B06 is due to the positions of galaxies in groups rather than the absolute numbers, and we refer the reader back to Fig. 3.

6 MAGNITUDE GAP

The magnitude ‘gap’ between the first- and second-ranked (and, indeed, lower ranked) galaxies within a group can be used as a predictor of group (or halo) age (von Benda-Beckmann et al. 2008), as the central galaxy tends to grow unceasingly with time via satellite accretion/stripping. This mechanism inevitably increases the magnitude gap. This process is controlled by feedback in the central galaxy (Section 2) and by infalling galaxies. Taken to its extreme, such an effect gives rise to the so-called ‘fossil groups’, which are groups with a magnitude gap greater than 2, most likely caused by a lack of recent galaxy infall on to the group (Vikhlinin et al. 1999; D’Onghia et al. 2005; Mendes de Oliveira et al. 2006; Sommer-Larsen 2006; Dariush et al. 2007; Sales et al. 2007; van den Bosch et al. 2007; Díaz-Giménez & Mamon 2010; however, see Zibetti, Pierini & Pratt 2009).

In Fig. 10, extreme right column, we compare the magnitude gap distribution between first- and second-ranked group galaxies in the suite of SAMs employed here. We show the distribution for all groups (top panel) as well as for the LGs, CGs and vCGs separately as we move downwards. The M_D06 model (and to a lesser extent, that of M_B07) shows a preferred magnitude gap of ~ 1 mag

between the two most luminous galaxies in the model groups (particularly in the CGs and vCGs). The D_B06 SAM predicts far more equal luminosity first- and second-ranked group galaxies. The difference in the distributions between the models is quite apparent, with a ‘turn over’ in the two Munich models, i.e. both are ‘flatter’ and ‘broader’ than the Durham models, for all group types and in all mass bins. Again, a significant difference in how the model’s galaxies evolve within dense environments has been highlighted by these observable characteristics.

Dariush et al. (2007; fig. 4a) show a comparable representation of the top-left panel of our Fig. 10, employing the Croton et al. (2006) SAM as applied to the Millennium Simulation (in the *R* band), and for a slightly different mass range, but effectively similar to what we have shown. Dariush et al. point out that the magnitude gap distribution of LGs in the Croton et al. (2006) model is similar to the $\ln \Lambda = 2$ theoretical model of Milosavljević et al. (2006), where $\ln \Lambda$ is the Coulomb logarithm that controls the merger rate. When the Croton et al. (2006) SAM is compared with the SDSS C4 catalogue (Miller et al. 2005), as is shown in fig. 4(c) of Dariush et al., the mismatch between small first- and second-ranked magnitude differences in the Munich SAM and the data become apparent, i.e. the SDSS C4 catalogue shows a magnitude difference distribution which prefers approximately equal luminosity functions for the first- and second-ranked galaxies in groups and clusters, more consistent with the Durham SAM predictions.

If we compare our result to the halo occupation distributions of van den Bosch et al. (2007), we find that we have far fewer fossils groups in the two high-mass bins for all three models but more for M_D06 groups in the lowest mass bin. A halo occupation distribution is a statistical model of the number and luminosity of galaxies occupying a dark matter halo of a given mass. As such, it is strongly related to the conditional luminosity function previously discussed, and serve as a base of comparison for the SAMs.

In order to make a fair comparison of the model predictions with the current observations, we take into account the selection effects inherent within the data. Specifically, the observational results (i) have a limited dynamic range of ~ 2 mag (Lin et al. 1996), driven by signal-to-noise ratio constraints applied to the lowest luminosity

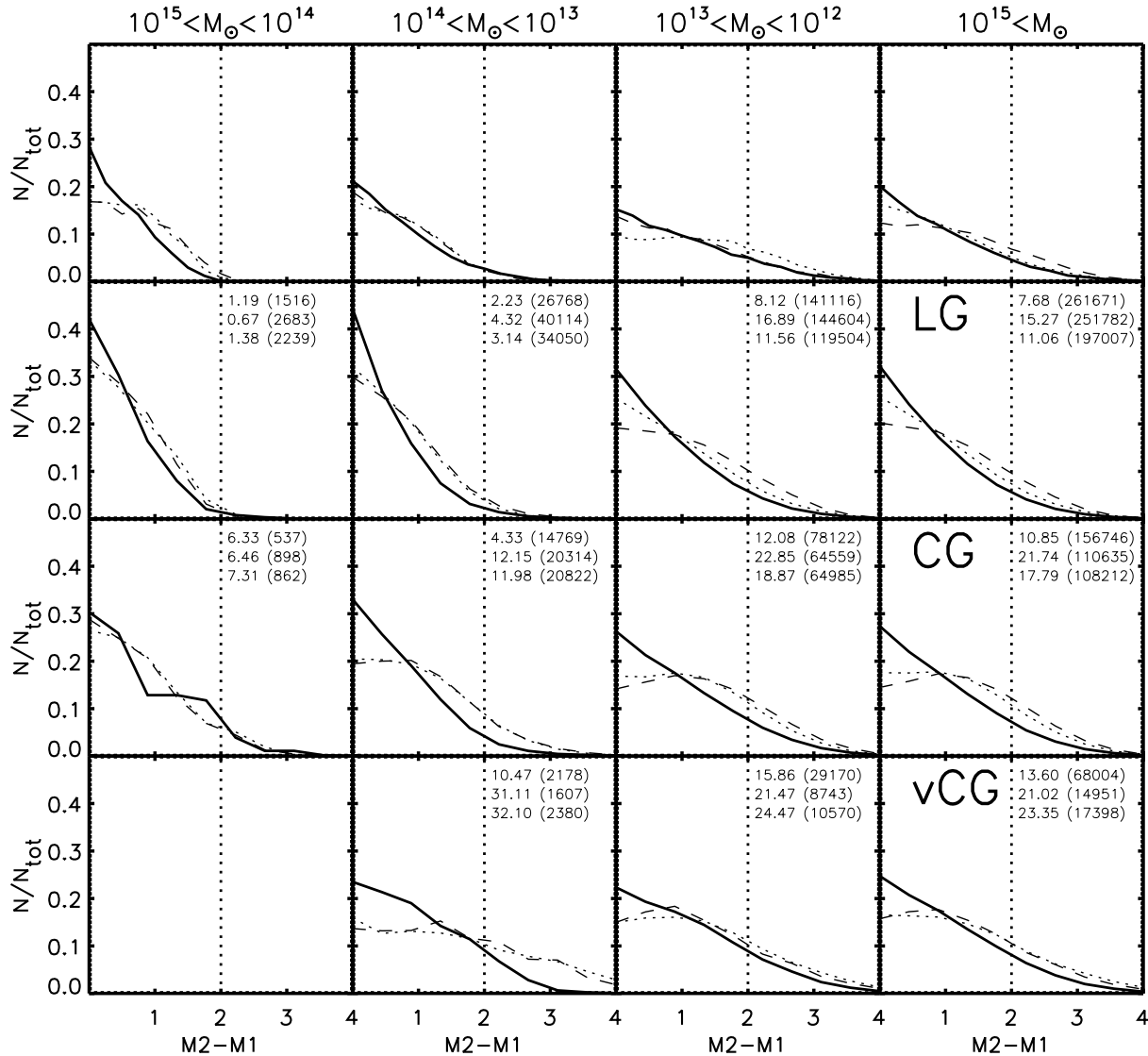


Figure 10. Conditional (mass-dependent) magnitude gaps between the first- and second-ranked galaxies for the SAMs included in this study. Solid, dashed and dotted lines are for D_B06, M_D06 and M_B07 groups, respectively. The top row is for halo-based groups divided by group mass and the extreme-right column is for all FoF groups regardless of mass; specifically, row 2 is for LGs, row 3 is for CGs and row 4 is for vCGs. The subsequent panels show the FoF-based groups broken down by halo mass. The vertical line shows the cut-off for Fossil groups (Sales et al. 2007). The numbers in each panel give the percentage of groups which are fossil systems, and, in brackets, the total number of groups in each mass bin. The first number is for D_B06, the second is for M_D06 and the third is for M_B07.

galaxies in the survey and (ii) discard groups that contain fewer than four galaxies within ~ 2 mag of the first-ranked galaxy. The Tago et al. (2008) groups were chosen for the comparison because the absolute r -band magnitude data were readily available. We have imposed comparable selection effects upon the models, and the impact upon the luminosity functions of the first- and second-ranked CG galaxies is shown in the right-hand panels of Fig. 11. The left-hand panels show that the turnover in the Munich models is no longer apparent, once a dynamic range of 2 mag is imposed upon the (theoretically, infinite) magnitude gap between the first- and fourth-ranked group galaxies. With these cuts, the models and data now lie closer to one another. However, the models produce a significant shortage of pairs with low-magnitude gaps for LGs and a higher population of groups with a magnitude gap of 1. This effect is more extreme in the Munich models but is still present in D_B06.

What is perhaps more interesting is that the dynamic range need only be increased to 3 mag for the models to diverge significantly, with the M_D06 model both ‘broadening’ and shifting to lower luminosity, relative to the distributions based upon the M_B07 and D_B06 SAMs, (right-most column of Fig. 10). Table 4 shows the populations of groups in the two extreme cases of small and large magnitude gaps for a dynamic range of 3 mag. The differences are very large between the Durham and Munich models. Certainly, observations with a higher dynamical range will provide a good test for differentiating the success of the SAMs within group environments. The relative success of the different manner that the SAMs implement physical processes such as AGN and SN feedback, and how these become important within group environments where satellite accretion modelling is also crucial, can then be better determined. One may also ask whether the assumption of separating central and satellite populations, whereby only the central galaxies experience

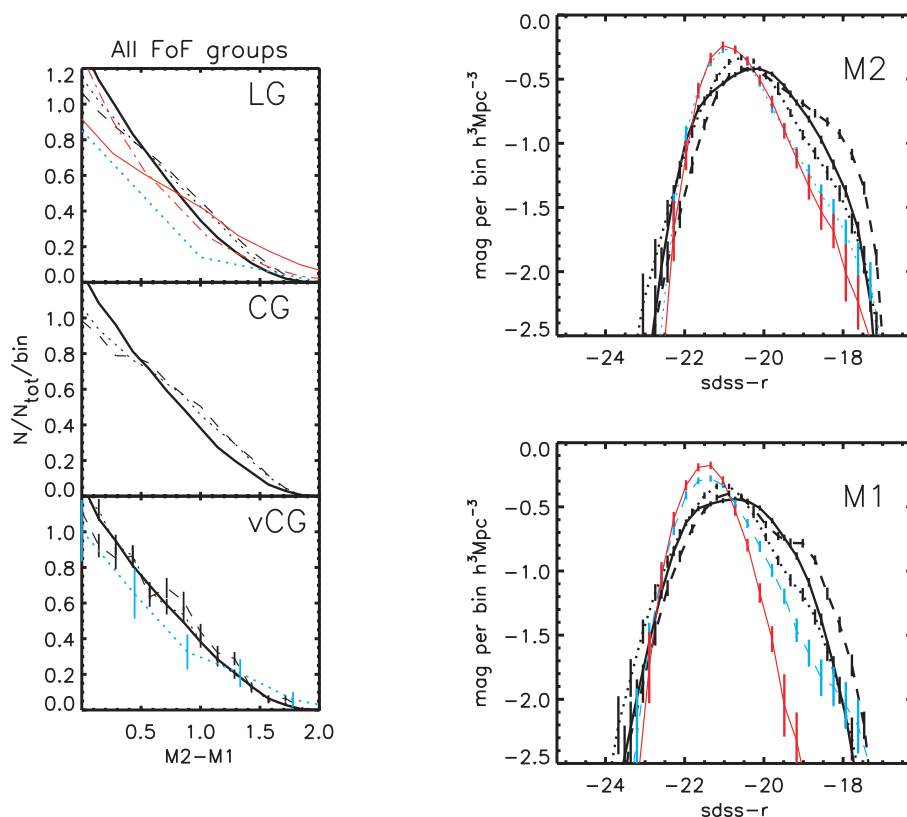


Figure 11. Left-hand column: distribution of the magnitude gap between the first- and second-ranked galaxies, normalized by the total number of groups in each sample. The thick solid, dashed and dotted lines are for D_B06, M_D06 and M_B07 models. The coloured lines show observational data. The top-left panel shows the Tago et al. (2008) groups (red dashed line), SDSS4_Y08 (red solid line) and Tucker et al. 2000 LGs (blue dotted line), the middle panel shows the results for CGs and the bottom-left panel shows the Allam & Tucker (2000) CGs (blue dotted line) along with vCGs. Poisson-counting uncertainties for each bin are reflected by the accompanying vertical bars. Right-hand column: the upper panel shows the luminosity function for the second-ranked LG galaxies and the lower panel shows the distribution of the first-ranked galaxies, and the observational data are taken from the Tago et al. (2008) groups (blue line) SDSS4_Y08 (red line). Data here have been restricted to mimic a survey in which the magnitude gap between the first- and fourth-ranked group galaxies is 2.

Table 4. Percentage of groups with the magnitude gap between the first- and second-ranked galaxies greater than 2 mag (top three rows) and less than 0.5 mag (bottom three rows).

Group	Gap	D_B06	M_D06	M_B07
LG	>2	10.8	20.6	15.2
CG	>2	14.9	28.4	23.8
vCG	>2	18.2	27.5	29.8
LG	<0.5	35.6	22.7	28.7
CG	<0.5	30.4	16.4	19.7
vCG	<0.5	27.5	17.8	18.7

mergers and no satellite galaxies grow while in the group environment, is appropriate when two galaxies of almost equal mass often exist within such environments.

The proportion of first-ranked (by luminosity) galaxies being centrals is sufficiently high to make the transition from the theoretical definitions of ‘central’ and ‘satellite’ galaxies into the observational regime of ‘brightest’ and ‘second brightest’ group galaxies, i.e. we can associate the brightest group galaxy with a central and the second-brightest galaxy with a satellite. This then allows us to plot the luminosity function of the first-ranked (M1) and second-ranked (M2) group galaxies, as shown in the right-hand panels of Fig. 11,

and associate the distributions in M1 with model centrals and in M2 with model (brightest) satellites. The first-ranked galaxy luminosity function of D_B06 is broader and flatter than those of the two Munich SAM variants; as expected, the M_B07 model galaxies are on average more luminous. For the distribution of the second-ranked galaxies, the M_D06 galaxies are on average ~ 1 mag less luminous than the Durham model galaxies, and the distribution is broader. The right-hand panels highlight that, although the global luminosity function of galaxies is well matched by observations, the distributions for the first- and second-ranked galaxies shown in Fig. 11 tend to be dimmer and wider than observations.

In Fig. 12, we demonstrate the impact of imposing a dynamic range of 3 mag between first- and fourth-ranked group galaxies; having done so, we find that the observations of SDSS4_Y08 match the model predictions of D_B06 remarkably well for LGs. This suggests that the Durham model, in this regime, provides a better match to empirical data than that of the Munich models.

7 CONCLUSIONS

By constructing luminosity functions of galaxy groups (ranging from loose to very compact) using variants of several leading SAMs, as applied to the Millennium Simulation, we have explored an astrophysical regime in which the SAMs have not been intercompared in great detail. Several obvious differences between the M_D06 and D_B06, i.e. loosely speaking, the Munich and Durham variants,

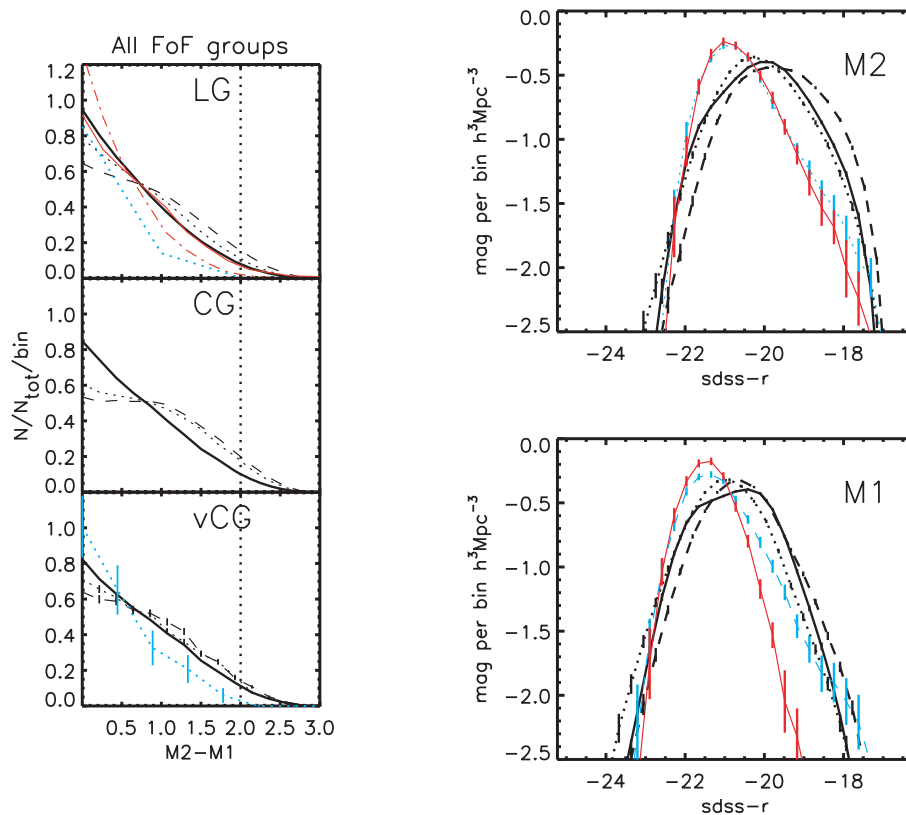


Figure 12. Left-hand column: distribution of the magnitude gap between first- and second-ranked galaxies, normalized by the total number of groups in each sample. The thick solid, dashed and dotted lines are for D_B06, M_D06 and M_B07 models. The coloured lines show observational data. The top-left panel shows the Tago et al. (2008) groups (red dashed line), SDSS4_Y08 (red solid line) and Tucker et al. 2000 LGs (blue dotted line), the middle panel shows the results for CGs and the bottom-left panel shows the Allam et al. (2000) CGs (blue dotted line) along with vCGs. Poisson-counting uncertainties for each bin are reflected by the accompanying vertical bars. Right-hand column: the upper panel shows the luminosity function for the second-ranked LG galaxies and the lower panel shows the distribution of the first-ranked galaxies, and the observational data are taken from the Tago et al. (2008) groups (blue line) SDSS4_Y08 (red line). In contrast with Fig. 11, data here have been restricted to mimic a survey in which the magnitude gap between the first- and fourth-ranked group galaxies is 3.

respectively, became apparent, including an intermediate-luminosity ‘wiggle’ in the M_D06 group luminosity functions not readily apparent when using the D_B06 SAM. We trace the origin of this wiggle to two competing effects resulting from the underlying physics within the M_D06 SAM – a steeper faint-end slope to the satellite luminosity function and a narrower distribution to the central galaxies luminosity function, most likely due to the lack of mass stripping in satellite galaxies without enveloping subhaloes, type 2 groups, and the particular formulation of the AGN in the Munich models. A systematic exploration of parameter space in the respective SAM may, however, be required to further isolate the cause of the difference.

Observations suggest that such a wiggle in the group luminosity function might exist (Weinmann et al. 2006), similar to that seen when applying the M_D06 SAM. However, these same observations tend to show a steeper magnitude gap (between the first- and second-ranked group members) distribution profile than that seen with any of SAMs, and we also see significant ‘flattening’ in the M_D06 gap distribution (i.e. a comparable likelihood for the first- and second-ranked galaxies to be of equal luminosity, as to have a 1 mag luminosity difference), a feature that is not consistent with the data sets described by Miller et al. (2005) or Dariush et al. (2007).

The models applied to the Millennium Simulation produce noticeably different galaxy group properties. The group luminosity functions diverge with increasing galaxy density meaning that, for

example, the cores of clusters in the various models have different properties, while the properties of the entire cluster will be more similar. As the same dark matter background was used in the three models, there are similar numbers of groups and clusters in the models, but according to our definitions, the denser structures are several times more common in the D_B06 model. The M_D06 model luminosity function shows a peak for the brightest galaxies that does not appear in the Durham models and is less evident in M_B07. The magnitude gap distributions of the models also differ with the Munich and Durham models demonstrating a different distribution at the small gap part of the distribution. All models show a shallower, wider magnitude gap distribution than the observations. This suggests that improvement in how the central/bright satellite luminosities are calculated is required. The designation of a single central galaxy which is modelled in a different manner to the other group members is a simplification which may need to be improved upon.

The existence of denser CG and vCG groups in the Durham models compared to the Munich sample suggests that the different merging time-scales and implementations of satellite accretion can have noticeable effects on the predictions of the models. Similarly, the fact that the Durham models show a shorter mean galaxy–galaxy separation indicates that these groups are denser. This suggests that merging time-scales are longer in the Durham groups. This is backed up by the luminosity function of groups because the evident ‘wiggle’ in the M_D06 groups appears to be due to a smaller

population of satellites and brighter centrals, which is a direct result of the rate at which satellite galaxies are accreted on to the central galaxy. However, while observations show a similar 'wiggle' in group luminosity functions, suggesting the shorter merging time is more physical, McConnachie et al. (2008) find fewer CGs in their field than in the SAMs, suggesting the merging time-scale should be even shorter. Contrastingly, the limited magnitude gap distribution indicates that the gap between central and satellite galaxies should be smaller, which may be due to additional physics that is not yet implemented in the models. Our analysis of the time-scales of merging shows that this is not the case, as satellites in both models last a similar amount of time. We emphasize, however, that there are more galaxies near the centre of a given group/cluster in the Durham models despite this. We suggest that this may be due to the additional time the M_D06 model takes in identifying subhaloes and reassigning the galaxy position of the central galaxy as the most bound particle in the (sub)halo. This may have the effect of keeping the galaxy out of the central region for longer. Although we do not find a noticeable difference in the merging times of galaxies in the two models, there is a substantial population of galaxies which do not merge. We can see this because more haloes merge in the Durham model but more galaxies merge in the Munich models. This serves to build up the number of satellites in the cluster, which fall into the cluster core, thus accounting for the observed difference in vCG population and galaxy-density distribution. This can explain the difference in the magnitude gap distribution because more galaxies merge with the central in the Munich model, reducing the number of satellites and making the central galaxy brighter.

ACKNOWLEDGMENTS

ONS acknowledges the support of the STFC through its PhD Studentship Programme. BKG and CBB acknowledge the support of the UK Science & Technology Facilities Council (STFC Grant ST/F002432/1) and the Commonwealth Cosmology Initiative; visitor support (PS-B, DK, AK and LVS) from the STFC (ST/G003025/1) is similarly acknowledged. PS-B acknowledges the support of a Marie Curie Intra-European Fellowship within the 6th European Community Framework Programme. AK and PS-B are supported by the Ministerio de Ciencia e Innovación (MICINN) in Spain through the Ramon y Cajal programme. The Millennium Simulation data bases used in this paper and the web application providing online access to them were constructed as part of the activities of the German Astrophysical Virtual Observatory. Access to the University of Central Lancashire's High Performance Computing Facility is gratefully acknowledged. We acknowledge the computational support provided by the UK National Cosmology Supercomputer, COSMOS. We thank the DEISA consortium, cofunded through EU FP6 project RI-031513 and the FP7 project RI-222919, for support within the DEISA Extreme Computing Initiative.

REFERENCES

Adelman-McCarthy J. K. et al., 2006, *ApJS*, 162, 38
 Adelman-McCarthy J. K. et al., 2007, *ApJS*, 172, 634
 Allam S. S., Tucker D. L., 2000, *Astron. Nachr.*, 321, 101
 Baldry I. K., Balogh M. L., Bower R. G., Glazebrook K., Nichol R. C., Bamford S. P., Budavari T., 2006, *MNRAS*, 373, 469
 Barton E., Geller M., Ramella M., Marzke R. O., da Costa L. N., 1996, *AJ*, 112, 871
 Baugh C. M., 2006, *Rep. Progress Phys.*, 69, 3101
 Benson A. J., Lacey C. G., Baugh C. M., Cole S., Frenk C. S., 2002, *MNRAS*, 333, 156

Bertone S., De Lucia G., Thomas P. A., 2007, *MNRAS*, 379, 1143(M_B07)
 Binney J., 2004, *MNRAS*, 347, 1093
 Blanton M. R. et al., 2003, *ApJ*, 592, 819
 Bower R. G., Benson A. J., Malbon R., Helly J. C., Frenk C. S., Baugh C. M., Cole S., Lacey C. G., 2006, *MNRAS*, 370, 645(D_B06)
 Cole S., Lacey C. G., Baugh C. M., Frenk C. S., 2000, *MNRAS*, 319, 168
 Croton D. J. et al., 2006, *MNRAS*, 365, 11
 D'Onghia E., Sommer-Larsen J., Romeo A. D., Burkert A., Pedersen K., Portinari L., Rasmussen J., 2005, *ApJ*, 630, L109
 Dariush A., Khosroshahi H. G., Ponman T. J., Pearce F., Raychaudhury S., Hartley W., 2007, *MNRAS*, 382, 433
 De Lucia G., Blaizot J., 2007, *MNRAS*, 375, 2
 De Lucia G., Springel V., White S. D. M., Croton D., Kauffmann G., 2006, *MNRAS*, 366, 499(M_D06)
 Díaz-Giménez E., Mamon G. A., 2010, *MNRAS*, 409, 1227
 Font A. S. et al., 2008, *MNRAS*, 389, 1619(D_F08)
 Geller M. J., Huchra J. P., 1983, *ApJS*, 52, 61
 González R. E., Padilla N. D., Galaz G., Infante L., 2005, *MNRAS*, 363, 1008
 Harker G., Cole S., Helly J., Frenk C., Jenkins A., 2006, *MNRAS*, 367, 1039
 Hatton S., Devriendt J. E. G., Ninin S., Bouchet F. R., Guiderdoni B., Vibert D., 2003, *MNRAS*, 343, 75
 Helly J. C., Cole S., Frenk C. S., Baugh C. M., Benson A., Lacey C., 2003, *MNRAS*, 338, 903
 Hickson P., 1982, *ApJ*, 255, 382
 Hickson P., Mendes de Oliveira C., Huchra J. P., Palumbo G. G., 1992, *ApJ*, 399, 353
 Lin H., Kirshner R. P., Shectman S. A., Landy S. D., Oemler A., Tucker D. L., Schechter P. L., 1996, *ApJ*, 471, 617
 Mateus A., 2008, *ApJ*, 684, 61
 McConnachie A. W., Ellison S. L., Patton D. R., 2008, *MNRAS*, 387, 1281
 McConnachie A. W., Patton D. R., Ellison S. L., Simard L., 2009, *MNRAS*, 395, 255
 Mendes de Oliveira C. L., Cypriano E. S., Sodré L., Jr, 2006, *AJ*, 131, 158
 Miller C. J. et al., 2005, *AJ*, 130, 968
 Milosavljević M., Miller C. J., Furlanetto S. R., Cooray A., 2006, *ApJ*, 637, L9
 Mo H. J., Yang X., van den Bosch F. C., Jing Y. P., 2004, *MNRAS*, 349, 205
 Navarro J. F., Frenk C. S., White S. D. M., 1996, *ApJ*, 462, 563
 Sales L. V., Navarro J. F., Lambas D. G., White S. D. M., Croton D. J., 2007, *MNRAS*, 382, 1901
 Schechter P., 1976, *ApJ*, 203, 297
 Shectman S. A., Landy S. D., Oemler A., Tucker D. L., Lin H., Kirshner R. P., Schechter P. L., 1996, *ApJ*, 470, 172
 Sommer-Larsen J., 2006, *MNRAS*, 369, 958
 Spergel D. N. et al., 2003, *ApJS*, 148, 175
 Springel V., White S. D. M., Tormen G., Kauffmann G., 2001, *MNRAS*, 328, 726
 Springel V. et al., 2005, *Nat*, 435, 629
 Tago E., Einasto J., Saar E., Tempel E., Einasto M., Vennik J., Müller V., 2008, *A&A*, 479, 927
 Tucker D. L. et al., 2000, *ApJS*, 130, 237
 van den Bosch F. C. et al., 2007, *MNRAS*, 376, 841
 Vikhlinin A., McNamara B. R., Hornstrup A., Quintana H., Forman W., Jones C., Way M., 1999, *ApJ*, 520, L1
 von Benda Beckmann A. M., D'Onghia E., Gottlöber S., Hoefl M., Khalatyan A., Klypin A., Müller V., 2008, *MNRAS*, 386, 2345
 Weinmann S. M., van den Bosch F. C., Yang X., Mo H. J., Croton D. J., Moore B., 2006, *MNRAS*, 372, 1161
 Yang X., Mo H. J., van den Bosch F. C., Jing Y. P., 2005, *MNRAS*, 356, 1293
 Yang X., Mo H. J., van den Bosch F. C., 2008, *ApJ*, 676, 248
 Zibetti S., Pierini D., Pratt G. W., 2009, *MNRAS*, 392, 525

This paper has been typeset from a \LaTeX file prepared by the author.